Renewable and Sustainable Energy Reviews 14 (2010) 598–614

Contents lists available at ScienceDirect

Renewable and Sustainable Energy Reviews

journal homepage: www.elsevier.com/locate/rser

An overview of phase change material slurries: MPCS and CHS

P. Zhang *, Z.W. Ma, R.Z. Wang

Institute of Refrigeration and Cryogenics, Shanghai Jiao Tong University, Shanghai 200240, China

ARTICLE INFO

Article history:
Received 2 July 2009
Received in revised form 31 July 2009
Accepted 22 August 2009

Keywords:
MPCS
CHS
PCS
Flow and heat transfer
Secondary loop

ABSTRACT

Phase change material slurries (PCS) can serve as both the heat transfer fluids and energy storage media, consequently, they are potentially applicable to the thermal systems, e.g., the secondary refrigeration and air conditioning loops, so as to improve the energy efficiency and to reduce the quantity of refrigerant used in the system. The design of the system using PCS needs the quantitative information about the thermal and fluidic behaviors of PCS. Here we provide an overview of the characteristics of two big groups of PCS, namely microencapsulated phase change material slurry (MPCS) and semi-clathrate hydrate slurry (CHS). The focuses are placed on the flow and heat transfer features and thermal properties, such as specific heat, viscosity and thermal conductivity. The suitable materials for making PCS are also discussed and compared based on the available data in the literature, and some examples of the applications of PCS are summarized as well.

Contents

1. Introduction

With the rapid development of the economy and human society, the energy and environmental issues have become more and more remarkable focuses because they will finally threat the survival of the human being if we do not take any actions to deal

* Corresponding author. Tel.: +86 21 34205505; fax: +86 21 34206814.
E-mail address: zhangp@sjtu.edu.cn (P. Zhang).

1364-0321/$ – see front matter © 2009 Elsevier Ltd. All rights reserved.
doi:10.1016/j.rser.2009.08.015

Nomenclature

A	parameter in Eq. (3)
B	parameter in Eq. (2)
C	specific heat capacity (kJ/(kg K))
d, D	diameter (m)
$\vec{e}$	shear rate (s^{-1})
f	Fanning friction factor
G	volumetric flow rate (m^3/s)
h	heat transfer coefficient (W/(m^2 K))
He	Hedstrom number
ΔH	enthalpy change (kJ)
l	length (m)
L	latent heat (kJ/kg)
k	thermal conductivity (W/(m K))
K, K'	fluid consistency coefficient
m	mass (kg)
M	molecular weight (g/mol)
n	flow behavior index
N	hydration number
Nu	Nusselt number
Pe	particle Pelect number
ΔP	pressure drop (Pa)
q	heat flux (W/m^2)
Q	heat (W)
r	radius (m)
R	radius (m)
Re	Reynolds number
Re'	the modified Reynolds number
Ste	Stephan number
T	temperature (K)
ΔT	temperature difference (K)
u	velocity (m/s)
v	mean velocity (m/s)
w	mass fraction (wt%)
W	power (W)
x	mass fraction
X	molar fraction

Greek letters

α	thermal diffusivity (m^2/s)
$\dot{\gamma}$	shear rate (s^{-1})
λ	Darcy friction factor
μ	viscosity (Pa s)
μ_a	apparent viscosity (Pa s)
μ_0	viscosity for Bingham equation (Pa s)
ρ	density (kg/m^3)
τ	shear stress (Pa)
τ_0	yield stress (Pa)
ϕ	volume fraction

Subscripts

0	initial
a	apparent
b	bulk
B	Bingham fluid
e	effective
f	fluid
H	hydrate
i	inlet
l	liquid
MR	Merzner and Reed
N	Newtonian
pcm	phase change material
P	particles
s	slurry
w	wall
x	distance from the inlet

with them. The countermeasures to the energy issue may include improving the energy efficiency, making use of the renewable energy and waste heat, and so on. One of the heavy energy consumers is the refrigeration and air conditioning; meanwhile, the ozone layer depletion and greenhouse gases emission of the environmental issue pose big concerns to the air conditioners and refrigerators where a huge amount of refrigerant is used, among which CFCs and HCFCs are the primary ones. The phase-out of CFCs and HCFCs according to the Montreal Protocol urges the researchers to find out the environment-friendly new substitutions for refrigerants or new technology to reduce the quantity of the refrigerant used in the systems. One approach to reduce the quantity of the refrigerant used in the circuit is to use the secondary refrigeration loop, which is responsible for distributing the cooling power. The main merits of such system are the quantity of the refrigerant involved is significantly reduced and the energy efficiency can be possibly improved by using the proper working medium in the secondary loop although the additional circulating device-pump is necessary.

The essence of the application of PCS to the secondary refrigeration loop is the introduction of the energy storage into the system, which releases the cooling power and enables that the primary refrigeration system does not need to work or works under a reduced load condition when the cooling power is needed, so that the electricity peak shaving can be readily realized. To increase the energy storage capacity, two-phase slurry fluid is preferred which is inspired by the fact that the latent heat storage associated with solid–liquid phase change is more efficient than the sensible heat storage of the single liquid phase. Apparently, selecting the appropriate working fluid for the secondary refrigeration loop plays a very critical role in such system.

In general, there are principally four kinds of two-phase fluids which can potentially be used as the secondary refrigerants [1], which have been named as the latent functionally thermal fluids (LFTF) [2]. Among these fluids, although ice slurry has been subjected to very intensive research and can be a very straightforward choice for the secondary refrigeration loop, the practical application is still limited due to the facts that there are still some weak points need to be solved, such as, the requirement for reliable ice slurry generator and ice concentration controller, and the requirement for improving the refrigerating efficiency of the ice slurry generation system because of significant subcooling necessary for ice nucleation. Recently, significant attention has been paid to the microencapsulated phase change slurry (MPCS) and semi-clathrate hydrate slurry (CHS), which have potential to be used in the secondary refrigeration and air conditioning loop systems. The main merits of MPCS and CHS over ice slurry are as follows: (1) the phase change temperature range is well fitted for air conditioning system, i.e. 5–12 °C, by properly selecting the phase change material (PCM) or by varying the salt concentration of the aqueous solution in the case of CHS; while the phase change temperature for ice slurry is 0 °C, lower than needed for the room conditioning; (2) the slurry particle size of MPCS or CHS can be smaller than that of ice slurry,

Table 1
Comparison of the typical materials used for PCS.

Material	Melting temperature (°C)	Density (kg/m^3)	Latent heat (kJ/kg)
MPCM ($C_{16}H_{34}$)	18	835/776 (solid/liquid)	237
CHS (TBAB, $(C_4H_9)_4NBr{\cdot}26H_2O$)	11.8	1080	193
Ice	0	920	333

which results in smaller frictional pressure loss for the same mass flow rate and less risk of clogging the transportation pipes; (3) the energy efficiency of the refrigerating system for MPCS and CHS is higher than that for ice slurry because of higher phase change temperature. The comparison of three typical materials for PCS is briefly shown in Table 1. Although the latent heat of ice associated with solid–liquid phase change is the largest, it is dimmed by the drawbacks stated above.

This paper presents a literature review of the research progress on the two-phase secondary loop by employing MPCS and CHS as the working fluids. The review has been arranged into two big sections regarding MPCS and CHS, respectively. Each section begins with the selection of the proper materials for PCS and is followed by the determining of the thermal properties of the slurry; the fluid flow and heat transfer characteristics of PCS are further discussed as they are very essential for the system design and optimization; at the end of each section, some practical applications of PCS to the refrigeration and air conditioning are mainly introduced and some problems are also proposed for further research in the summary.

2. Microencapsulated phase change material slurry (MPCS)

2.1. The material and fabrication of microencapsulated phase change material (MPCM)

Microencapsulation is a kind of tiny particles (about 0.1–1000 μm in diameter) in which the core material is enveloped by a thin layer of shell. The core material can be solid, liquid, gas or even the mixture, and the shell material is generally natural or synthesized polymer of about several micrometers in thickness. This technology has been widely used in such fields as medicine, chemical engineering, etc. Recently, it has been extended to the preparation of the microencapsulated phase change material (MPCM), by which several inherent problems, such as low thermal conductivity, big volume change of the organic PCM and the thermal instability of the inorganic PCM, can be possibly overcome. When MPCM is dispersed into the carrier fluids, it forms a kind of two-phase suspension-MPCS and the application of MPCS to the energy system becomes very simple. Although the carrier fluid should have high thermal conductivity and large specific heat capacity, water is generally used as it has no obvious negative effect on the compatibility of MPCM and is easy to handle.

There are several methods which can be used to produce microencapsulated particles, such as spray-drying and fluidized bed process for physical approaches; and there are also chemical processes which can be used for microencapsulation, such as simple and complex coacervation, in situ polymerization and so on. The in situ chemical process is often used in the laboratory since it can produce the microencapsulated particles with good quality. Although the diameter of MPCM depends on the fabrication method, the typical size is in the range of micrometers. Shown in Fig. 1 are the typical SEM pictures of MPCM [3]. It can be seen from the surface morphology that the shape of MPCM is uniformly spherical and the surface is very smooth without edges and dents, which implies that fluidity is good if the MPCM is dispersed into the carrier fluids, such as water.

The intensive effort for developing MPCM can be traced back to two or three decades ago in America [4]. However, much attention was not paid to the application of MPCM to such fields as thermal system, building material, textile application and so on, until recently.

There are many kinds of MPCMs which can potentially be used for the secondary loop purpose. However, before it can be used, one kind of MPCM should generally meet several requirements for both core and shell materials, which include the follows: (1) core material: suitable temperature range, large latent heat, reasonable thermal conductivity, low volume change, low reactivity, and so on; (2) shell material: good sealing tightness, endurance, good elastic strength, water and fire resistance, and so on. It is actually almost impossible to find a MPCM which can meet all the above requirements.

The core material used for MPCM is commonly organic material considering the technical feasibility, and the shell material can be urea–formaldehyde resin, melamine–formaldehyde resin and even some other resins depending on the chemical process involved. It is obvious that the paraffin is the best candidate as the core material due to its stable chemical properties, suitable thermal properties and low cost. The thermal properties of the paraffin depend on the carbon atom number in the molecule, and the melting temperature ranges very wide from −57 °C for n-Octane (C_8H_{18}) to 80 °C for n-Tetracontane ($C_{40}H_{82}$). The latent heat associated with the solid–liquid phase change of paraffin is quite large. Table 2 shows the technical data for n-alkanes which are the main contents of the paraffin. However, the heat transfer is always limited by its low thermal conductivity during heat retrieval. One solution is making the paraffin into microparticles by utilizing microencapsulation technology.

Alkan et al. [5] have prepared MPCM with docosane as the core material and polymethylmethacrylate (PMMA) as the shell

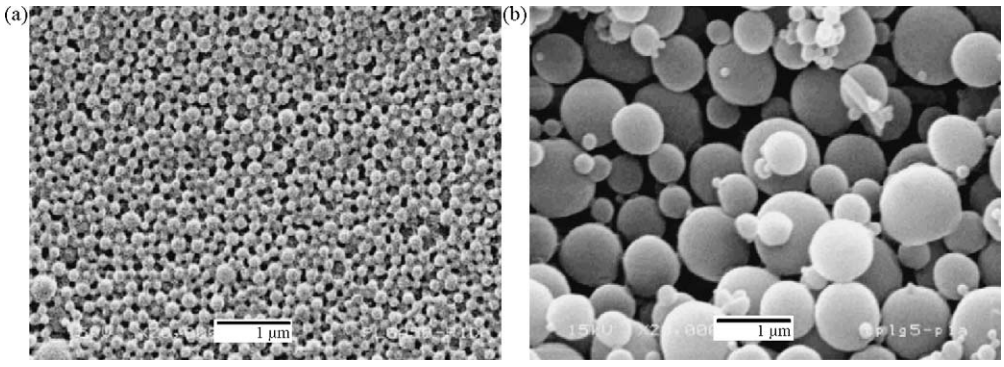

Fig. 1. Typical SEM pictures of MPCM made by different methods [3]. (a) By spray-drying and (b) by coacervation.

Table 2
The technical data for n-alkanes. (The values of the thermal conductivity and density may vary with temperature).

Carbon Number	Name Formula (mol weight)	Melting Temperature (°C)	Latent Heat (kJ/kg)	Thermal Conductivity (W/(m K)) solid/liquid	Density (kg/m^3) solid/liquid
C(8)	n-Octane C_8H_{18} (114.23)	−57 (−56.5)	181	−/0.128	−/703.6
C(10)	n-Decane $C_{10}H_{22}$ (142.28)	−30	201	−/0.1349	−/730
C(12)	n-Dodecane $C_{12}H_{26}$ (170.34)	−9.5 (−12)	216	0.21/0.14	−/750
C(14)	n-Tetradecane $C_{14}H_{30}$ (198.39)	6	226	0.21/0.15	825/771
C(16)	n-Hexadecane $C_{16}H_{34}$ (226.44)	18	237	0.21/0.151	835/776
C(18)	n-Octadecane $C_{18}H_{38}$ (254.50)	28	243	0.35/0.151	840/778
C(20)	n-Eicosane $C_{20}H_{42}$ (282.55)	37	247	0.23/0.151	856/780
C(22)	n-Docosane $C_{22}H_{46}$ (310.61)	44.5	249	0.22/0.151	864/780
C(24)	n-Tetracosane $C_{24}H_{50}$ (338.66)	52 (51)	255	0.25/0.15	897/774

material by using emulsion polymerization. The characterizations of MPCM were also carried out by using SEM and FT-IR for the morphology and chemical contents. Differential Scanning Calorimetry (DSC) and Thermo-Gravimetric Analysis (TGA) were applied for determining the thermal properties and thermal stability. The results indicated that the MPCM was very suitable for thermal energy storage for space heating purpose since its phase change temperature was around 40 °C.

A systematical investigation of the synthesis of MPCM with paraffin wax with high melting temperature as the core material and urea–formaldehyde as the shell was carried out by Jin et al. [6]. They focused on the effects of the synthesis conditions on the morphology and thermal properties of MPCM and found that the particle size of MPCM decreased from 20 to 5 μm as the amount of the emulsifier increased. The quantity of the shell material used in the synthesis was very crucial in deciding the toughness of the shell of MPCM. It was shown that the MPCM particles made under certain conditions might experience leakage when they were subjected to the thermal cycles with the temperature higher than the melting temperature. Consequently, the core material (paraffin wax) re-coalesced, which implied the failure of the MPCM particles. The pipe might be clogged if the leakage of MPCM occurs since the core material may stick together to form big lumps. However, this could be avoided by properly increasing the amount of the shell material used in synthesis process. DSC tests indicated that the melting temperature of MPCM was little affected and the latent heat decreased almost linearly with the core content.

A simple method to make MPCM has been proposed by Ai et al. [7]. The particularity of this method is to use casein as the protein multilayer to protect the microparticles from re-coalescencing before MPCM is finally stabilized. The fabrication process is shown in Fig. 2. They used n-hexadecane as the core material. It was shown that the casein was very effective in protecting the agglomeration of emulsion. Further measurements indicated that the melting temperature of MPCM was increased and latent heat of MPCM was smaller than the bulk material which they attributed to the presence of the impurity. The decrease of the latent heat was always a drawback of MPCM because of the presence of the shell.

Zou et al. [8] fabricated the MPCM by the interfacial polycondensation using hexadecane as the core material. It was found that the average diameter of MPCM was about 2.5 μm, and the latent heat was drastically decreased to 66.09 J/g compared to 236 J/g of pure hexadecane; while the melting temperature was not seriously affected.

MPCMs are generally synthesized with melamine–formaldehyde (MF), urea–formaldehyde (UF) or gelatin–formaldehyde as the shell materials. However, formaldehyde is harmful to the health, the remnant of which should be reduced to meet the limitation by the standard when MPCM is used for textile. Li et al. [9] prepared the melamine–formaldehyde (MF) prepolymer by incorporating formaldehyde once and melamine three times. Urea was used to remove the remnant of formaldehyde after the in situ polymerization finished. The morphology of the fabricated MPCM was investigated for different dropping rate of MF prepolymer into the n-octadecane emulsion. The characterization showed that the average diameter was about 2.2 μm with very narrow range and the MPCM contained 59 wt% of n-octadecane with the enthalpy of 144 J/g. The measurement showed that the remnant of

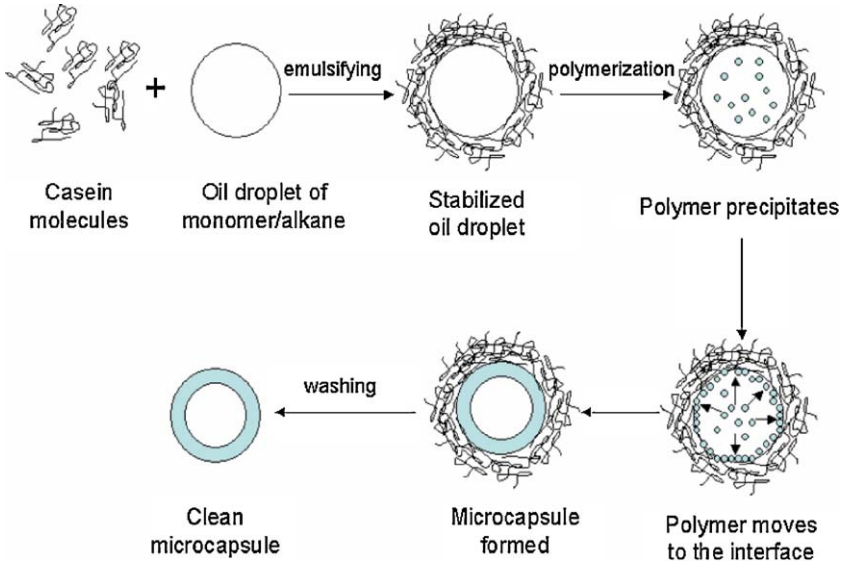

Fig. 2. A simple method for making MPCM proposed by Ai et al. [7].

formaldehyde was only 67.1 mg/kg, which implied that MPCM had the potential application for the textile.

In addition to the paraffin used as the core material, coco fatty acid mixture can also be the candidate for MPCM. Özonur et al. [10] used inexpensive natural coco fatty with the melting temperature in the range of 22–24 °C as the core material and several kinds of possible shell materials were tested by the coacervation techniques. Results indicated that gelatin–gum Arabic was the best shell material in microencapsulation, and the diameters of the fabricated MPCMs were around 1000 μm. The MPCM would be very cheap by using the proposed cheap core and shell materials, which opened a new way to reduce the cost of MPCM.

A lot of effort has been devoted to the determination of the thermal properties of MPCM which are obviously very much different from those of the bulk materials. In the energy storage and transportation applications, the thermal properties including latent heat, subcooling degree, melting temperature, viscosity, etc. are the most important ones.

Subcooling is always a serious problem in PCM research and application. One of the drawbacks of MPCM is the possibility of increasing the subcooling degree, which should be effectively suppressed before MPCM can be used as the energy storage and transportation medium, because the subcooling will drastically deteriorate the system performance and reduce the energy efficiency, for example, increasing the refrigerating load and reducing the efficiency of the refrigerating system for chilling MPCM in air conditioning applications.

Alvarado et al. [11] experimentally characterized the thermal behavior of the bulk and microencapsulated n-tetradecane by using DSC. The subcooling degree was specially studied and compared, and several methods were tried to reduce the subcooling degree. Silica fume as the nucleating agent was test and the results showed that its presence could significantly suppress the subcooling for the bulk material, while 0.2 wt% of silica fume was not effective for MPCM, which indicated that a suitable nucleating agent is necessary for the future study. A comparative study by using a more stable nucleating agent-tetradecanol with 1–4 wt% was carried out, and it was showed that 2 wt% of tetradecanol was already very effective in suppressing subcooling. However, the mass fraction of the nucleating agent should not be too high because it will reduce the latent heat significantly with increasing the concentration.

There are several kinds of materials which can be used as the nucleating agents to suppress the subcooling of MPCM. Fan et al. [12] prepared three kinds of MPCMs (n-octadecane as the core material) with sodium chloride, 1-octadecanol and paraffin as the nucleating agents, respectively. It was revealed that the subcooling could be effectively suppressed by increasing the concentration of the nucleating agent to 6, 9 and 20 wt% for sodium chloride, 1-octadecanol and paraffin, respectively. However, addition of sodium chloride and 1-octadecanol as the nucleating agents had the drawbacks on the morphology and dispersibility of MPCM, which resulted in rough shell surface and agglomeration. Nevertheless, addition of paraffin to the core material had little effect on the morphology and dispersibility of MPCM. This point may be very important because rough surface of MPCM will increase the circulating pumping power which is undesirable to the practical application for the energy storage and transportation.

Table 3 shows the summary of the core and shell materials, nucleating agents and the size distribution of MPCM. Some information is from the commercial available products, and the most are the laboratory-scale test samples.

2.2. Fundamental features of MPCS

2.2.1. Thermal properties of MPCS

When the MPCM is dispersed into the carrier fluid, e.g. water, a kind of suspension named as microencapsulated phase change slurry (MPCS) is formed. Due to the relatively large surface area to volume of MPCM, better heat transfer performance can be achieved. Thus, MPCS can serve as both the energy storage and heat transfer media, in addition, the agglomeration of MPCM can be avoided due to the encapsulation. It is obvious that, however, the heat transfer and fluid flow characteristics are very important for the MPCS system design. As a kind of suspension, the thermal properties of MPCS are different from those of the bulk PCM

Table 3
Summary of the core and shell materials, nucleating agents and size distribution of MPCM.

Reference	Core material	Shell material	Nucleating agent	Size distribution (μm)	Comments
Alkan et al. [5]	Docosane	Polymethylmethacrylate (PMMA)		0.16 (average)	
Jin et al. [6]	Paraffin wax	Urea–formaldehyde		5–20 (depending on synthesis condition)	
Ai et al. [7]	n-Hexadecane	Polystyrene		3–15	Latent heat was drastically decreased due to the impurity
Zou et al. [8]	Hexadecane	Shell was formed by interfacial reaction between TDI and EDA		1.26–10 (2.5 average)	Latent heat was drastically decreased
Li et al. [9]	n-Octadecane	Melamine–formaldehyde (MF)		2.2 (average)	Formaldehyde was reduced
Özonur et al. [10]	Coco fatty	Gelatin–gum Arabic		1000	Very cheap
Alvarado et al. [11]	n-Tetradecane	gelatin	0.2 wt% silica fume, 2 wt% tetradecanol, etc.	90–125, (100 average)	0.2 wt% of silica fume (not effective for MPCM) tetradecanol with 1–4 wt% (effective)
Fan et al. [12]	n-Octadecane		Sodium chloride, 1-octadecanol and paraffin		
Zhang et al. [13]	8.8 vol% cyclohexane and 91.2 vol% n-octadecane	Urea–melamine–formaldehyde		0.4–5.6	
Wang et al. [16]	1-Bromohexadecane ($C_{16}H_{33}Br$)	Amino plastics		2.0–31.7 (10.1 average)	
Inaba et al. [20]	n-Docasane, n-tetradecane			15, 1.5	
BASF (Micronal® DS 5000, 5007)	Paraffin wax	PMMA		5	Commercially available
Microtek	Paraffin wax	Polymer		5–40	Commercially available

materials and carrier fluids, which are very essential for the evaluation of the flow and heat transfer characteristics of MPCS. In the following context, brief discussion of the determination of the thermal properties of MPCS is first introduced, which mainly include the thermal conductivity, viscosity and specific heat.

In general, the thermal conductivity of the static MPCS with low volume fraction can be evaluated by Maxwell's equation formulated as

$$k_s = k_f \times \frac{2k_f + k_P + 2\phi(k_P - k_f)}{2k_f + k_P - \phi(k_P - k_f)} \quad (1)$$

where k_s and k_f are the thermal conductivities of the bulk slurry and carrier fluid, and ϕ is the volume fraction of MPCM. The thermal conductivity of the MPCM particle k_P can be estimated by a correlation describing composite sphere feature [14]. Under the flowing condition, the effective thermal conductivity is generally higher than that predicted by Maxwell's equation due to the interaction between the particle and fluid. Then, a general correlation summarized in reference [15] can be applied depending on the particle Peclet number

$$\frac{k_e}{k_s} = 1 + B\phi Pe_P^m \quad (2)$$

where k_e is the effective thermal conductivity of the PCS, $Pe_P = \vec{e} \cdot d^2/\alpha_f$ is the particle Peclet number, $\vec{e}$ is the shear rate, α_f is the thermal diffusivity, and the values for B and m depend on the particle Peclet number. In general, the thermal conductivity of MPCM particles is not very large and needs to be enhanced. It has been proposed that a certain amount of nano-particles are added to PCM so as to enhance the thermal conductivity of MPCM as in the case of nano-fluids.

The viscosity of MPCS is critical in determining the pressure drop when MPCS is used to transport energy. When the volume fraction of MPCM is less than 25%, the MPCS is generally considered as the Newtonian fluid. The viscosity is generally measured by using viscometer, and the results [16,17] indicated that the MPCS showed the Newtonian fluid feature and the apparent viscosity was about 1.5–10 times of the water as the mass fraction of MPCM increased from about 5 to 30%. The MPCS can be treated as the homogeneous fluid at low volume fraction, and the apparent viscosity of the slurry can be estimated by the following equation [18] which includes the effect of the interactions between MPCM particles, carrier fluid and even the tube wall.

$$\frac{\mu_s}{\mu_f} = (1 - \phi - A\phi^2)^{-2.5} \quad (3)$$

where A is a parameter depending on the shape and rigidity of the particles. The pressure drop can be calculated by the equation for the single phase flow by using the apparent viscosity, however, the effect of non-Newtonian rheology will be more evident as the volume fraction increases beyond 30%. It has been demonstrated that MPCS shows Newtonian rheology in the most studied volume fraction range, nevertheless, it displays mostly non-Newtonian rheology for clathrate hydrate slurry even at low volume fraction, which will be discussed in detail in Section 3.

The specific heat of the MPCS without phase change can be simply estimated from the mass and energy balance approach which can be formulated as

$$C_{P,s} = w_{pcm}C_{pcm} + w_{shell}C_{shell} + w_f C_f \quad (4)$$

where w_{pcm}, w_{shell} and w_f are the mass fractions of the PCM, shell and carrier fluid, respectively, and $w_{pcm} + w_{shell} + w_f = 1$. However, when the phase change is involved in the estimation of the heat transfer performance, the effect of the latent heat should be properly treated and an effective specific heat is used which can be written as if all the MPCM has been melted

$$C_e = C_{P,b} + \frac{w_{pcm}L}{\Delta T} \quad (5)$$

where ΔT is the phase change temperature range.

2.2.2. Flow and heat transfer characteristics of MPCS

Charunyakorn et al. [15] proposed a theoretical model to study the forced convection heat transfer of MPCS, in which several dimensionless parameters, like the bulk Stephan number, particle volume fraction, modified Peclet number and so on, are included. The results showed that the bulk Stephan number and particle volume fraction were the most important parameters which affected the heat transfer of MPCS.

Goel et al. [19] conducted experiments to investigate the laminar forced convection heat transfer of MPCS in order to provide the useful information which could be directly used by those who were not involved in this field. The Reynolds numbers studied were about 200 and 1000. The experimental results indicated that about 50% reduction in wall temperature could be realized by using MPCS compared with single phase fluid flow and the Stephan number, defined in the following equation, was the most dominant parameter in the convection heat transfer similar to the results of Charunyakorn et al. [15].

$$\mathrm{Ste} = \frac{C_{P,s}|q_w R/k_s|}{\phi_p L\rho_P/\rho_s} \quad (6)$$

Due to the temperature control application purpose, either heat transfer coefficient or Nusselt Number was not chosen to characterize the heat transfer performance. A dimensionless wall temperature defined as $\theta_{wx} = (T_{wx} - T_i)k_s/(q_w D)$ was used to represent the wall temperature. Shown in Fig. 3 is one typical result under different Stephan numbers when the volume fraction of MPCM is 10% and diameter is about 100 μm. Although the comparison of the experimental results to theoretical ones of Charunyakorn et al. [15] was made, it was found that the agreement was only qualitatively well due to the complexity of the problem. The effects of the other influential parameters, like volume fraction, diameter of MPCM and the homogeneity of MPCM particles, have also been investigated and discussed.

Inaba et al. [20] studied the heat transfer characteristics of MPCS composed of different sized particles in a circular tube. MPCM with a nominal size of 15 μm (n-docasane as the core material) in diameter was blended with smaller sized MPCM of 1.5 μm (n-tetradecane as the core material) in diameter. The flow of MPCS exhibited smaller friction factor than that of the pure water as the drag-reduction additives which could reduce the flow resistance was added. The MPCS with different sized particles

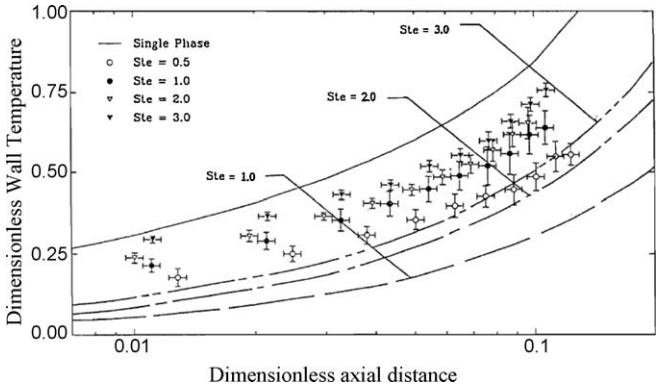

Fig. 3. Comparison of the experimental and theoretical results for the dimensionless wall temperature [19], volume fraction 10%, Re = 200, d = 100 μm.

showed better heat transfer performance than that with mono-sized particle, which was due to the microconvection around the particles.

The advantage of application of MPCS to the energy storage and transportation is that the phase change with latent heat is involved and thus the effective specific heat of the fluid is remarkably increased which results in the heat transfer enhancement. However, one has to take the pumping power into consideration when putting MPCS into the practical application. Inaba et al. [20] found that the flow drag reduction could be achieved in the turbulent flow regime, while the pressure drop was increased in the laminar flow regime in the case of higher mass fraction of larger sized particles. Thus, the ratio between the heat Q transported by MPCS (including both latent heat and sensible heat) and the pumping power W of the circulating pump has to be investigated. They showed experimentally that Q/W for MPCS was larger than that for water in the turbulent flow regime, while in the laminar flow regime, Q/W decreased from larger than that for water to less than that for water as increasing the fraction of the larger MPCM particles, as shown in Fig. 4. This fact indicated that both the energy transportation and pumping power should be simultaneously considered in the application of MPCS.

MPCM should be endurable before it can be put into long-term operation, because it might be broken by the circulating pump. Alvarado [21] showed that MPCM (n-tetradecane as the core material) with the diameter of smaller than 10 μm could be endurable and impact-resistant by using cavity pump to do the durability test. The pressure drop and heat transfer characteristics were also experimentally measured. It was showed that the pressure drop of MPCS at low mass fraction was much smaller than that of water, while the differences decreased as the mass fraction increased, which might imply that there was a possible drag reduction effect of MPCS. The heat transfer coefficient of MPCS reached its peak when the temperature was close to the melting temperature of n-tetradecane, which indicated that additional specific heat caused by the phase change enhanced the heat transfer. However, the heat transfer coefficient of MPCS was generally smaller than that of water under the same condition, which might be attributed to the turbulence reduction and smaller thermal conductivity of MPCS. The using of the enhanced tube might be effective in enhancing the heat transfer.

Wang et al. [16] presented a comprehensive study of the heat transfer of MPCS in circular tube. They used 1-bromohexadecane ($C_{16}H_{33}Br$) as the core material and amino plastics as the shell material for microencapsulated particles. The experimental heat transfer coefficient was compared with Gnielinski correlation for single phase flow and it was found that the correlation for single phase flow could not properly describe the heat transfer of MPCS.

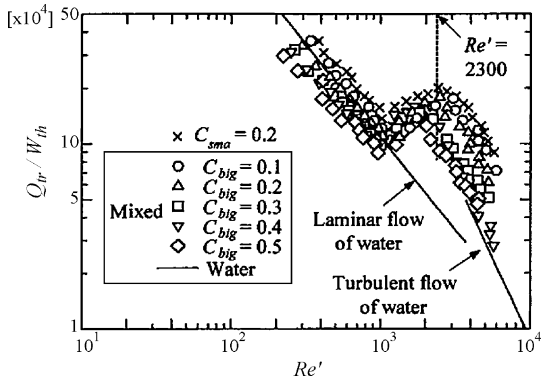

Fig. 4. Variation of the ratio of the heat Q transported by MPCS to the pumping power W with Re' [20], where Re' is the modified Reynolds number based on power viscosity law, C in the figure is the mass fraction.

Although there were several empirical heat transfer correlations for solid–liquid two-phase slurry flow reported in the literature, however, they were only applicable to the heat transfer of slurry without phase change. In the case of MPCS, the authors finally proposed their own correlations based on the experimental data by including the Stephan number. The comparison of the experimental data and correlation showed that the relative errors for the laminar and turbulent heat transfer were within ±10%. It was concluded that the heat transfer was enhanced for MPCS and the average Nusselt number was about 1–2.5 times higher than for the pure water in the case of the turbulent flow.

The phase change problem of MPCM attracted quite a lot of attention because of its fundamental importance. Zhao et al. [22] carried out a parametric analysis of the heat transfer enhancement of the laminar flow of MPCS in the circular tube under the constant wall temperature condition. They adopted the definition of the modified local heat transfer coefficient and modified Nusselt number to avoid unreasonable inflexion of the local heat transfer coefficient and Nusselt number. Totally, six factors including the Stefan number, volume fraction of MPCM particles, ratio of the particle radius to tube radius, subcooling, dimensionless phase change temperature range and the bulk flow Reynolds number were taken into consideration in the analysis. The analytical results indicated that the Stephan number, volume fraction and size of the MPCM particle were the most important influential factors for the heat transfer enhancement, and the enhancement up to 4 times could be achieved by employing MPCS as the working fluid.

MPCM can be used to increase the energy storage density of the heat storage system. A mathematical model was developed to study the thermal behavior of a MPCS latent heat storage system on the basis of the energy conservation and heat transfer [23]. It was revealed that the convective heat transfer coefficient between the MPCM particles and the carrier fluid (water) played a very critical role in the charging and discharging cycles. Some other influential factors including MPCM mass fraction and particle diameter were also investigated. These results were very helpful in optimizing the thermal system although some simplifications were made in the analysis.

Yamagishi et al. [24] carried out quite detailed tests of the MPCM particles with the core material of n-tetradecane and n-dodecane (with the melting temperatures at 5.0 and −13.5 °C as reported by the authors, respectively). Although the above two bulk materials did not have evident subcooling degrees, it was found from the test results that the subcooling was quite significant as the diameter of the particle decreased, which could be even as large as up to 15 °C, as shown in Fig. 5. The heterogeneous nucleation is generally preferred than the homogeneous nucleation because the former occurs at higher temperature. In order to solve the subcooling problem, the nucleating agent of 1-tetradecanol for n-tetradecane was applied, which effectively decreased the subcooling and reduced the cooling time. The tolerance against the shear force induced by pumping is very essential for practical application. Breakage tests were carried out for different sized particles, which revealed that the smaller particles could survive the test. MPCS with high volume fraction generally has quite large apparent viscosity which consequently increases the pressure drop and pumping power. However, the drag-reduction surfactants can be used to reduce the pressure loss in the tube. Shown in Fig. 6 is the variation of the friction factor with the Reynolds number for MPCS with the surfactant, which evidently shows that the flow characteristics display the similar feature to that of the Newtonian fluid.

It can be seen that it is very useful to disperse MPCM into the carrier fluids to form MPCS for the thermal storage and management application. The convective heat transfer coefficient is generally larger than that of the single phase fluid flow because

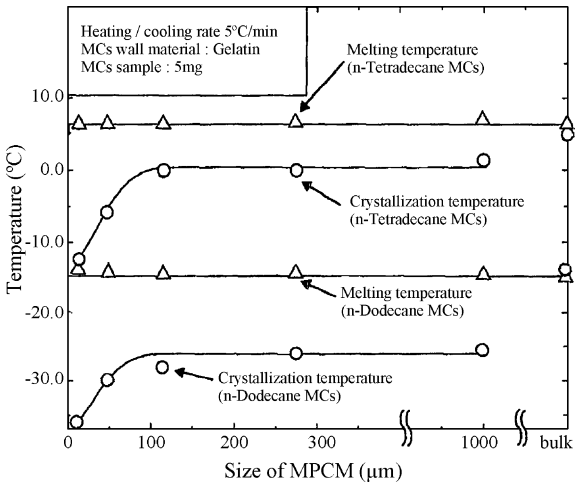

Fig. 5. Variation of the melting and crystallization temperatures with the size of MPCM [24].

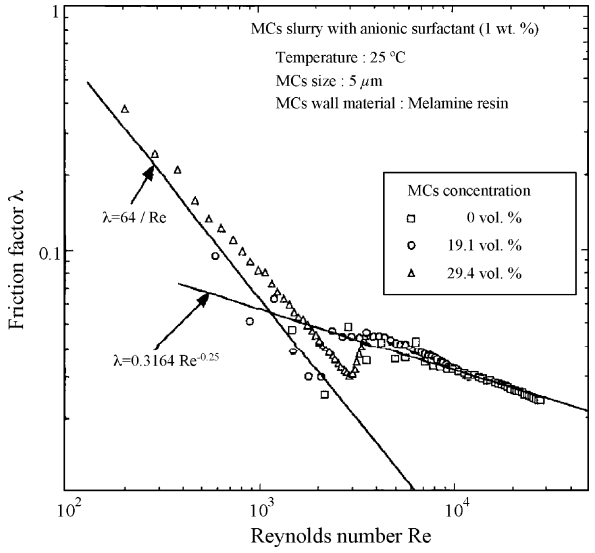

Fig. 6. Variation of the Darcy friction factor with the Reynolds number [24].

of the increase of the specific heat by the phase change. The pressure drop can be generally predicted by the single phase flow correlation when the volume fraction of MPCM is not very large, and the pressure drop can be effectively reduced by using the drag-reduction additives in the case of high volume fraction of MPCM.

2.3. Application of MPCS to the thermal systems

The application of MPCS to the thermal systems mainly includes its using in the thermal storage and transportation system, and in the thermal controlling aspects and so on. One typical example is the secondary loop for refrigeration and air conditioning.

An assessment of the performance of the embedding MPCS energy storage and evaporative cooling into a cooled ceiling system was carried out by Wang et al. [25]. The core material of MPCM was hexadecane with a melting temperature of 18.1 °C, which enabled the possible integration into the cooled ceiling system usually working at 14–20 °C. In the research, MPCS was only used for the energy storage, but not used as the working fluid for the secondary loop. The results indicated that the annual energy saving potential up to 80% could be achieved in north-western China.

The comparative studies of the energy charging and releasing performances of PCM in an annular space were carried out by Balikowski and Mollendort [26] by using Climsel 28 (ordinary PCM) and microencapsulated Thermasorb 83. It was found that the heat transfer rate of latter was about 25% higher in the charging period and also 20% higher in the discharging period, which indicated that MPCM could significantly increase the heat storage/retrieval rates.

Griffiths and Eames [27] have conducted experimental tests by using MPCS (products of BASF) as both the energy storage and transportation media in a cooled ceiling system. It was concluded from four months-long experiments that 40 wt% MPCS could effectively reduce the flow rate while maintaining the constant cooling temperature, thus the total pumping power was reduced compared to the large flow volume of the water.

Fossett et al. [28] has proposed to use the MPCM embedded heat sink instead of a solid aluminum plate as the passive heat sink for the avionic application. The advantage of using MPCM in the heat sink over the bulk PCM lies in eliminating the volume change during melting or solidification. Both the experimental and analytical investigations on a heat sink with a size of 12.7 cm × 22.9 cm in basement and 2.54 cm in thickness were carried out, and 270 g MPCM with the melting temperature close to the temperature range of the cooling application was used. The heating load of 90 W was applied to the heat sink and was lasting for 10 min. It was found that the temperature of the MPCM heat sink could be well maintained below the safety temperature of the electronic device at 71 °C in 10 min at an initial temperature of 52 °C which was about 10 °C smaller than the melting temperature of MPCM. However, it was only one minute when the temperature of the heat sink without MPCM reached 71 °C under the same initial condition. The analytical results agreed quite well with the experimental ones. This technology is very useful for the design of the light airborne heat sink.

A quite large-scale application of MPCS to cooling in Narita airport of Tokyo was described by Shibutani [29], which was implemented by the co-operation between Narita airport and Mitsubishi Heavy Industries Ltd. The initiation of the project was motivated by the phase-out of refrigerants R11 and R22. If the system was re-charged with R134a and R123, there would be the decrease of the cooling capacity and performance without replacing the chiller system. Thus, there was insufficient cooling power supply in the daytime. However, this problem could be overcome by incorporating the cold storage system into the existing chiller system. The temperatures of the chilled water in the supply and return pipes of the existing system were 5 and 12 °C, respectively. The MPCM with the average diameter of 2 μm and phase change temperature between 7 and 8 °C was therefore selected for the cold storage system. Shown in Fig. 7 is a typical temperature variation of the MPCM used for the cold storage and cold release, in which an evident phase change part could be easily observed and the significant increase of the cold storage density was achieved compared to the chilled water. A storage tank with the volume of 970 m^3 was installed onsite and was coupled to the chiller through a plate heat exchanger. The system operation showed that the cold storage density was 67 MJ/m^3 with MPCS, larger than 21 MJ/m^3 with cold water, although much smaller than 167 MJ/m^3 with ice. While the energy efficiency and running cost for the former two cases were similar, better than the ice storage.

There are already commercial available MPCMs in the market with the typical products from BASF and Microtek company. Gschwander et al. [30] dispersed BASF MPCMs, as shown in Table 3, into water to form MPCS and studied the durability after pumping for several weeks at a rate of 800 cycles/day. The long-term tests

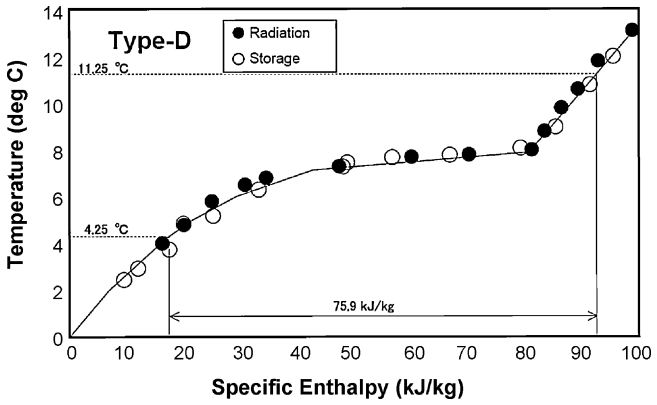

Fig. 7. Temperature variation of the MPCM used for the cold storage and cold release [29].

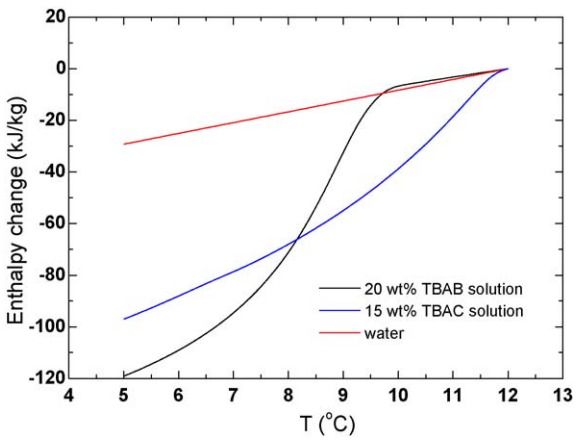

Fig. 8. Comparison of the enthalpy changes of the TBAB CHS, TBAC CHS and water in the temperature range of 5–12 °C, the base point is taken at 12 °C.

indicated that the centrifugal pump was suitable for pumping MPCS and caused less damage to the shell of MPCS. Their initial test indicated that MPCM might be broken when transported through pump, while this could be tackled by increasing the thickness of the shell and reducing the diameter, although it resulted in less melting enthalpy of MPCS. The pressure drop and temperatures were recorded in the test in order to evaluate the performance of MPCS, and the thermal tests implied that MPCS was especially advantageous for the applications with a small temperature difference.

Many investigations have demonstrated that MPCM can be readily dispersed into carrier fluids to form MPCS, which can be used as both the heat transfer and energy storage media. Nevertheless, much effort is still needed to improve the performance, such as specific heat, thermal conductivity and durability, and to understand the flow and heat transfer characteristics of MPCS, so as to promote the applicability at the industrial scale.

3. Clathrate hydrate slurry (CHS)

The other big category of the PCS is clathrate hydrate slurry (CHS). Although clathrate hydrate itself has already been subjected to the intensive study in the field of chemistry, its application to the energy storage and transportation is still very new and at its early stage. Clathrate hydrate is generally produced under high pressure and low temperature condition, however, some semi-clathrate hydrate, for example, semi-clathrate hydrates of quaternary ammonium salts (e.g. tetrabutylammonium bromide, TBAB in abbreviation) can be formed under the condition of one atmosphere pressure and room temperature. Due to the fact that a phase change with the latent heat up to several hundred kJ/kg is associated with the formation and dissociation of the semi-clathrate hydrate, it is possible to be employed in the energy storage and transportation application. For example, the cold storage capacity of TBAB CHS was about 2–4 times larger than that of the cold water in the temperature range of 5–12 °C depending on the mass fraction of the hydrate crystals in the slurry, which implies that the flow rate can be decreased and therefore the pumping power can also be reduced. Shown in Fig. 8 is the comparison of the enthalpy changes of the TBAB CHS, TBAC CHS and water in the temperature range of the air conditioning application, i.e., 5–12 °C. The enthalpy changes of CHS are calculated from the DSC curves and it is obvious that the enthalpy change of CHS is much larger than that of the water.

Although the research of the semi-clathrate hydrates of quaternary ammonium salts can be traced back to several decades ago, it does not draw the intensive attention until recent years. This section provides the review of the studies of CHS used as PCS, focusing on the fundamental properties of CHS, the generation, flow and heat transfer characteristics and the applications.

3.1. Fundamental properties of clathrate hydrate crystals

3.1.1. Structures and shapes of hydrate crystals

Clathrate hydrates of tetraalkylammonium salts with simple anions (such as halides, sulfate, formate, etc.) were firstly reported by Fowler et al. in 1940 [31]. Later, many researchers carried out a lot of investigations on clathrate hydrates, most of which were focused on the crystal data and structure refinement from chemical aspects. Nonetheless, some thermal properties were also reported.

Clathrate hydrate is a chemical compound in which the water molecules ("host") form lattice structures and molecules of another substance ("guest") fill the lattices. It is known that salt anions are bound to water molecules through hydrogen bonds and form a water-anion framework in the semi-clathrate hydrate [32]. In the following context, TBAB is mainly discussed as an example because its clathrate hydrate was subjected to the most intensive studies. Even under one atmosphere pressure and room temperature condition, TBAB in water can form a semi-clathrate hydrate in which TBAB molecules are both the host and guest, as shown in Fig. 9. There are still small dodecahedral empty cages in TBAB clathrate hydrate. Hence, TBAB clathrate hydrate is able to uptake, store and separate small gas molecules under different thermal conditions, which have spawned a lot of researches on this topic recently [33,34].

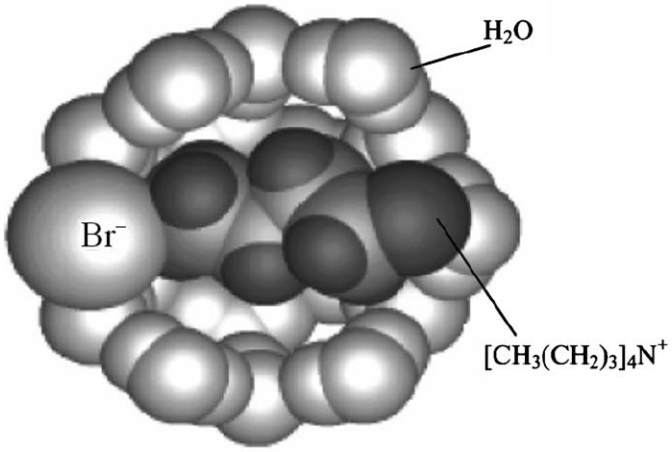

Fig. 9. Molecular structure of TBAB semi-clathrate hydrate.

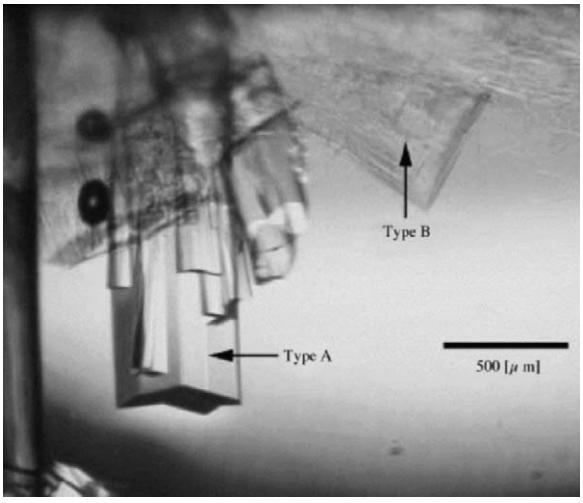

Fig. 10. Two types of TBAB hydrate crystals [35].

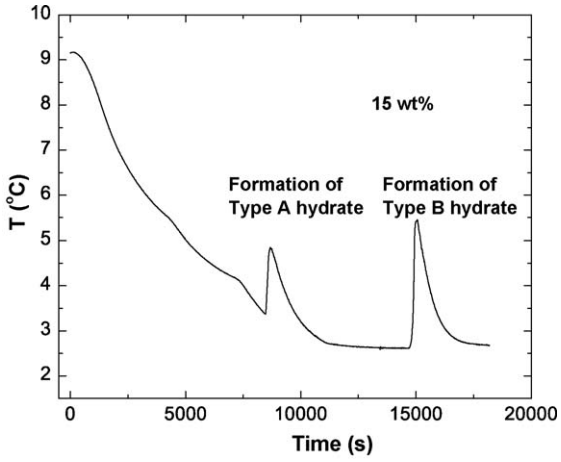

Fig. 11. Two temperature ascents in the cooling down of TBAB aqueous solution.

TBAB CHS appears white and is a kind of solid–liquid suspension like ice slurry. There are generally two different types of TBAB hydrate crystals, as shown in Fig. 10, and their existences have been confirmed by the facts that the temperature ascends twice during the cooling down of TBAB aqueous solution. Shown in Fig. 11 is the cooling curve of TBAB aqueous solution with two temperature spikes which indicate two different phase changes corresponding to the formation of two different hydrate crystals with different transmittances, refractive indices and crystal morphologies. Type A is columnar shape and type B is an irregular form composed of thin crystals [35]. Shimada et al. [36] observed the growth of TBAB hydrate crystals using a digital high definition microscope, and showed that the growth of TBAB hydrate was highly dependent on the interfacial kinetics. More information about structures and shapes of TBAB clathrate hydrate crystals, etc. can be found in the references [32,37]. Similar to TBAB, Rodionova and Manakov [38] also observed two types of clathrate hydrates of tetrabutulammonium fluoride (TBAF), and they isolated both hydrate crystals from the aqueous solution and their appearances are shown in Fig. 12 with tetragonal structure and cubic structure, respectively.

3.1.2. Phase diagram of CHS

Through cooling down the salt aqueous solution with strong agitation, hydrate crystals will nucleate in the liquid. Hydrate crystals do not appear until the temperature reaches a certain degrees lower than the crystallization temperature due to the subcooling phenomenon. Once the nucleation occurs in the subcooled aqueous solution, the subcooled state will gradually disappear due to the release of the latent heat in the exothermic process, and the mixture temperature will ascend to the phase change temperature of the original aqueous solution. If the original salt concentration of the solution is equal to the salt mass fraction in hydrate crystal (e.g. 40.8 wt% for TBAB·26H_2O), the salt concentration in liquid phase will remain constant even after the hydrate crystals form. Then the hydrate crystals will keep forming until all solution is crystallized, therefore the CHS temperature remains nearly constant due to the latent heat released. Based on this phenomenon, the congruent concentration, the corresponding melting temperature and the hydration number can be determined. Other melting temperatures at incongruent concentrations can also be determined from the cooling curve. However, after the hydrate crystals form, the salt concentration in liquid phase changes and lower temperature is needed to sustain the crystallization, so the CHS temperature can not be kept constant but decreases due to the cooling.

The heating in DSC test was used by many researchers to determine the melting temperatures and latent heats of hydrate crystals while the cooling was not suitable due to the subcooling phenomenon. Typical DCS curves are shown in Fig. 13. One of the important factors that affect the measurement accuracy is the heating rate which has been investigated in many studies. Nakayama [37] and Rodionova and Manakov [38] used the heating rate of 0.5 °C/min in the measurement, while Yamazaki et al. [39] applied the heating rates of 2 °C/min and 0.1 °C/min in the case of low salt concentration. It is generally accepted that higher heating rate results in a better measuring sensitivity, but the penalty is that the resolution will be decreased.

According to Oyama et al. [35], DSC was not suitable for determining the phase diagram of TBAB clathrate hydrates,

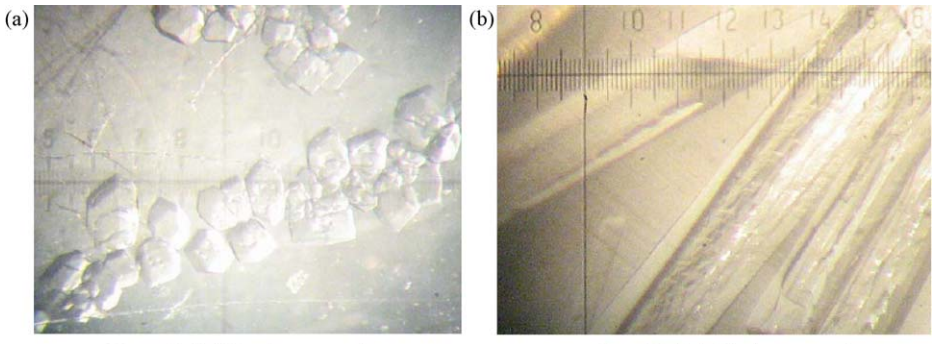

Fig. 12. Two types of TBAF hydrates crystals [38].

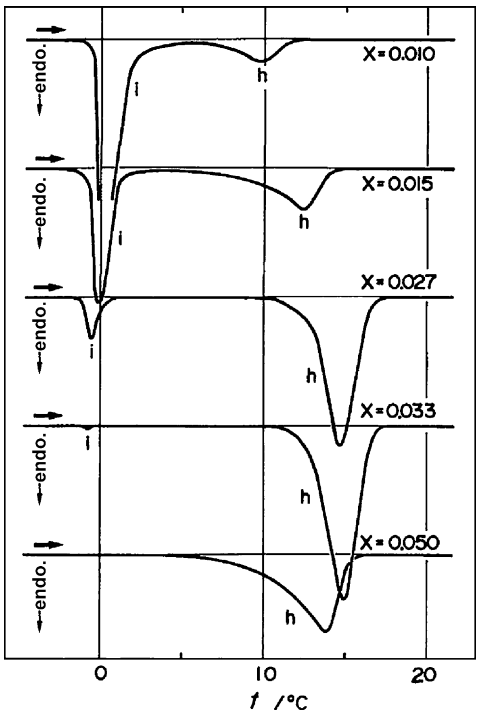

Fig. 13. Typical DSC heating curves of CHS [37], *X* in the figure is molar fraction.

because there are two kinds of TBAB hydrate crystals and their melting temperature peaks are too close to be separated. They measured the melting temperatures of these two types of hydrate crystals by two different techniques. For type A hydrate, the common method was used and a heating rate of 2 °C/h was applied for CHS; for type B hydrate, they grew and separated the crystals and raised the temperature at a step of 0.1 °C, and observed the crystals by a digital CCD microscope to determine the dissolving temperature, which was indicated by the surface of crystals becoming visibly rough.

Fig. 14 shows the phase diagrams of four typical clathrate hydrates which have been studied as the thermal energy storage media except tetrabutylammonium chloride (TBAC). A lot of information about CHS can be obtained from the phase diagram. Salt mass fraction in the liquid phase x_l can be determined from the corresponding CHS temperature T on the phase diagram, then hydrate mass fraction x_H and volume fraction ϕ can be calculated by the following equations:

$$x_{\mathrm{H}} = \frac{x_0 - x_{\mathrm{l}}}{x_{\mathrm{N}} - x_{\mathrm{l}}} \tag{7}$$

$$\phi = \frac{x_{\mathrm{H}}/\rho_{\mathrm{H}}}{x_{\mathrm{H}}/\rho_{\mathrm{H}} + (1 - x_{\mathrm{H}})/\rho_{\mathrm{l}}} \tag{8}$$

where x_0 is the initial salt mass concentration in the aqueous solution, x_N is the salt mass fraction in the hydrate crystal, ρ_H and ρ_l are the densities of the hydrate crystal and liquid, respectively.

3.1.3. Thermal properties of hydrate crystals and CHS

Thermal properties of the hydrate crystal are essential for understanding the fundamental features of clathrate hydrate and further application. Given in Table 4 are the thermal properties of TBAB, TBAF, TBAC and TME hydrate crystals, including the hydration number, melting temperature, density, latent heat, specific heat and thermal conductivity.

The latent heat and specific heat of the clathrate hydrate are usually determined from the DSC curves, in which the effect of the ice should be carefully considered. Nakayama [37] analyzed the cooling curves of TBAC aqueous solution measured by DSC, and the hold point which was after the formation of hydrate and before the formation of ice was determined to separate the enthalpy change

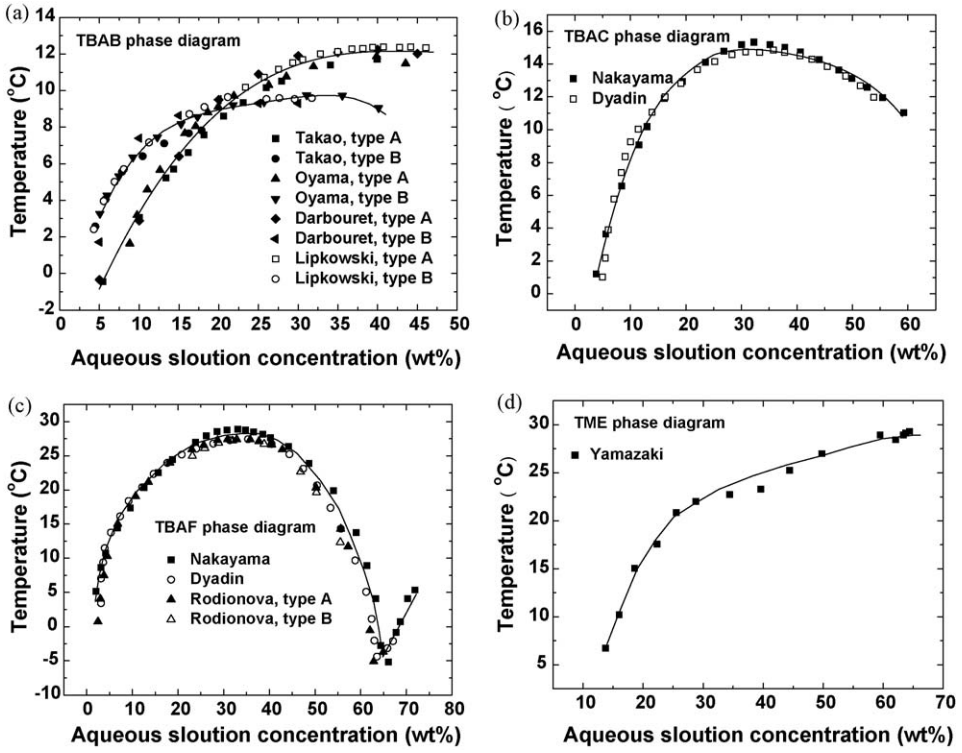

Fig. 14. Phase diagrams of four CHS (a) TBAB hydrate, hydrate number N_{type_A} = 26, N_{type_B} = 36 (38 according to Oyama [35]); (b) TBAC hydrate, N = 30 [37]; (c) TBAF hydrate, N = 30 according to Nakayama [37], N = 29 according to Dyadin [40], N_{type_A} = 30 and N_{type_B} = 33 according to Rodionova [38]; (d) TME hydrate, N = 3.

Table 4
Characteristics of TBAB/TBAC/TBAF/TME hydrate crystals.

	Authors	Hydration number	Melting temperature (°C)	Density (kg/m^3)	Latent heat (kJ/kg)	Specific heat (kJ/(kg K))	Thermal conductivity (W/(m K))
TBAB	Lipkowski et al. [32]	24/26/32/36/2/3	12.4/12.2/11.7/9.5/–/–				
	Oyama et al. [35]	26/38	12.0/9.9		193.2/199.6	[a]1.86–2.61/2.0–2.54	
	Darbouret et al. [48]	26/36	12.3/9.6	1082/1067			
	Hayashi et al. [49]						
	Ogoshi and Takao [55]	26/36	11.8/–	1082/1030	193/205	2.22/–	0.42/–
TBAC	Nakayama [37]	30	15.0		200.7		
	Dyadin and Udachin [40]	29.7/32.1	15.0/14.7	1034/1029			
TBAF	Nakayama [37]	30	28.3		229.7		
	Rodionova and Manakov [38]	29.7/32.8	27.7/27.2		223.1/240.5		
	Dyadin and Udachin [40]	28.6/32.3	27.4/27.2	1057/1035			
TME	Yamazaki et al. [39]	3	30.0	1120/1090	218	[b]2.75/3.58	[c]0.65/0.21

[a] Between −20 and 0.2 °C.
[b] At 10 and 50 °C.
[c] At 22 and 56 °C, respectively.

for ice and hydrate, as shown in Fig. 15. The author obtained the total enthalpy change ΔH_1 and the hydrate enthalpy change ΔH_2, then the latent heat L and hydration number N can be calculated by:

$$L = \frac{\Delta H_2}{m - (\Delta H_1 - \Delta H_2)/L_{ice}} \quad (9)$$

$$N = \frac{(m_{H_2O} - (\Delta H_1 - \Delta H_2)/L_{ice})/M_{H_2O}}{m_{salt}/M_{salt}} \quad (10)$$

Another way of using DSC to measure the latent heat of the hydrate crystal directly was proposed by Oyama et al. [35]. The authors separated the two types of TBAB hydrate crystals from the aqueous solution, and these crystals were further stabilized by quenching in liquid nitrogen and then were measured by using DSC directly. Therefore the sole latent heat without the interference of the enthalpy change of solution was obtained. The key point of this method is the purity of the hydrate crystals because ice would more or less adhere to the hydrate crystals. Hydrate crystals growing at their congruent concentration will be in high purity, however, not all hydrates are congruently crystallized, such as type B TBAB hydrate, etc. Oyama et al. took the influence of the ice remnant on the surface of type B TBAB hydrate crystals into consideration, and obtained the final results of the latent heats for TBAB hydrate crystals. Moreover, the specific heats of TBAB hydrate crystals were determined from the same DSC results. It was considered that the larger latent heat and specific heat of type B TBAB clathrate hydrate are the results of larger hydration number.

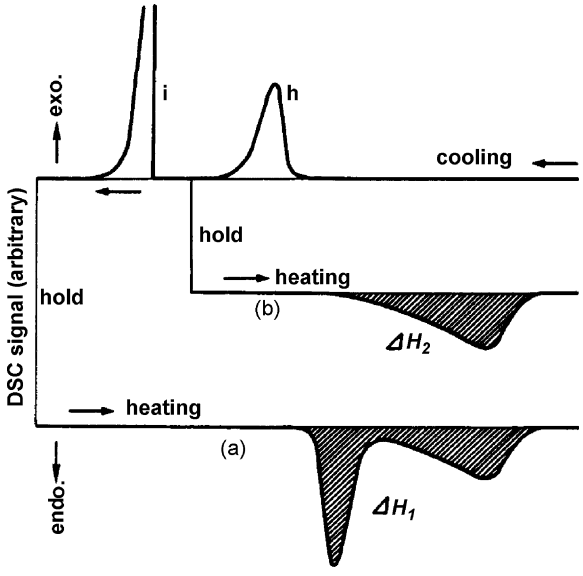

Fig. 15. The method used to determine the latent heat of hydrate on DSC curve [37].

Thermal conductivity of CHS was rarely reported in the literature, however, it can be calculated by Maxwell's equation shown in Eq. (1). And the approaches depicted in the sections for determining the thermal conductivity of MPCS can also be applicable to CHS.

3.1.4. TBAB clathrate hydrate combined with gas molecules

Semi-clathrate hydrate is able to uptake, store and separate low molecular weight gases, which opens a new way for the gas storage and transport. Arjmandi et al. [41] studied the equilibrium data of hydrogen, methane, nitrogen, carbon dioxide and natural gas in TBAB clathrate hydrate, which showed that these double hydrates were more stable than the single TBAB hydrate. The dissociation enthalpy of gas hydrate is generally larger than that of salt clathrate hydrate, for example, 374 kJ/kg for CO_2 hydrate. Usually, the equilibrium pressure of gas hydrate is very high. However, tetrahydrofuran (THF) or TBAB can be added to reduce the equilibrium pressure of gas hydrate, as shown in Fig. 16, which is obviously more favorable for application.

Delahaye et al. [42] investigated the effects of THF on the equilibrium pressure decrease and dissociation enthalpy enhancement of CO_2 hydrate. And 3.8–15 wt% THF was added to water,

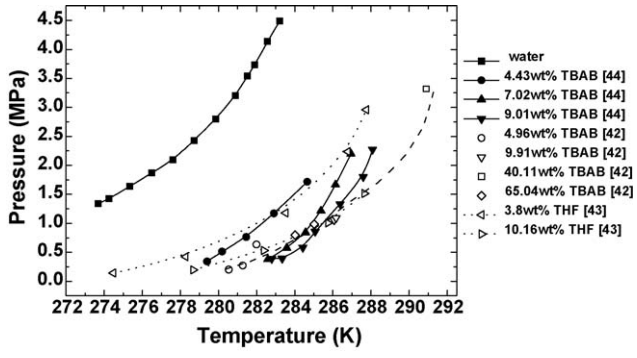

Fig. 16. Equilibrium pressure reduction of CO_2 hydrate with TBAB/THF in water [42–44].

which showed that the equilibrium pressure of CO_2 hydrate has been reduced by about 80% and the dissociation enthalpy of the THF + CO_2 double hydrate in the unit of kJ/mol was nearly two times of that of single CO_2 hydrate.

Lin et al. [43] applied the differential thermal analysis (DTA) to measure the dissociation enthalpy of TBAB + CO_2 double hydrates. The composition of hydrate formed with 9.01wt% TBAB + CO_2 is $2.51CO_2 \cdot TBAB \cdot 38H_2O$ and its dissociation enthalpy is 313.2 kJ/kg, smaller than that of the single CO_2 hydrate, but larger than that of TBAB clathrate hydrate (about 200 kJ/kg). Li et al. [44] tested the equilibrium data of TBAB solution combined with CH_4, which showed that the equilibrium pressure was reduced drastically by 52–96% compared to the single CH_4 hydrate and the equilibrium temperature was increased by 4–17 °C compared to that of TBAB clathrate hydrate.

3.2. Generation of clathrate hydrate crystals

The basic steps to generate the hydrate crystals from the aqueous solution include supersaturation, crystals nucleation and growth. Following these three steps, attrition, agglomeration and ripening are needed to make the hydrate particles to take the prescribed shape and size. Hydrate can be formed only if there is a sufficient driving force, therefore supersaturation state is necessary. Usually, supersaturation can be achieved by decreasing the temperature to lower than the crystallization temperature or by changing the pressure to shift the equilibrium temperature. Under the chemical potential difference, water molecules and salt ions collide with each other and combine together to form small clusters which are the initial nuclei and the formation of the nuclei relieves the supersaturation. It is difficult to initialize the crystallization in the clear aqueous solution; otherwise, the subcooling degree needed for the homogeneous nucleation is very large. However, heterogeneous nucleation occurs in most cases, in which the dust particles in the solution or on the surface of the blade and container will help the formation of the nuclei.

Similar to MPCS, subcooling phenomenon is unwanted due to the excess energy consumption in the hydrate generation. Several methods have been proposed to suppress the subcooling degree, such as adding nucleating agent, agitation, ultrasonic vibration and so on, which are similar to the methods used in the case of MPCM. Takao et al. [45] suggested to drop fine nucleating particles into the solution to act as the nuclei to suppress the subcooling, which showed that the subcooling degree was reduced from 14 °C to less than 2 °C. Although this method can be used to accelerate the nucleation, the nucleating agent particles should be prevented from being circulated in the entire system, therefore, additional devices are needed to reclaim the nucleating agent particles which make the system complicated.

On the other hand, the addition of some nucleating agents, such as ethylene glycol and propylene glycol, will change the melting temperature of the clathrate hydrate. Wu et al. [46] added 6–8 wt% NaCl to 40.5 wt% TBAB solution, which results in decreasing the melting temperature from near 12 °C to 6–8 °C. Therefore, this high concentration solution can be useful for application due to the decrease of the melting temperature. In general, the hydrate crystal easily nucleates and grows on the container wall, and then the heat transfer performance or energy storage capacity may be deteriorated due to the gradual increase of the thickness of the hydrate crystal layer. Daitoku and Utaka [47] used the scraper to detach the solid layer of TBAB hydrate adhering on the wall which would reduce the heat transfer performance, and the different morphology of hydrate crystals on the wall before and after scraping was reported.

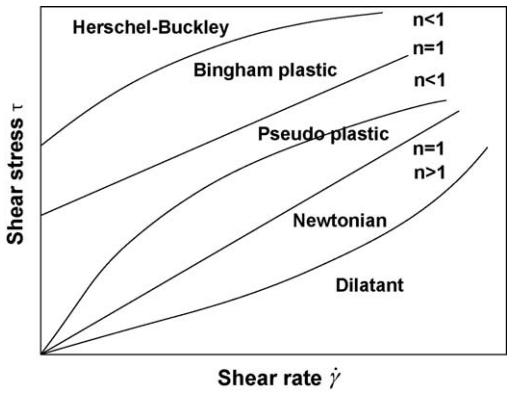

Fig. 17. Typical flow curves of purely time-independent non-Newtonian fluids.

3.3. Flow characteristics of CHS

3.3.1. Fluidity of CHS

Different from MPCS, CHS is usually considered as non-Newtonian fluid due to its solid–liquid two-phase mixture feature. However, it can possibly be treated as Newtonian fluid when the solid fraction is very small.

Darbouret et al. [48] suggested that the traditional viscometers were not suitable for measuring the viscosity of the solid–liquid suspension due to the density segregation phenomenon. If the solid fraction further depends on the temperature, like CHS, the measurement is even more difficult due to the temperature controlling problem. Consequently, many researchers determined the apparent viscosity of suspensions, such as ice slurry, microemulsion, CHS, etc., by the shear rate and shear stress which are obtained by measuring the volumetric flow rate and differential pressure drop of slurry flowing in a horizontal tube.

Simple non-Newtonian fluid is a time-independent viscous fluid, and the shear stress is a function only of shear rate but it is more complicated than Newtonian fluid. Fig. 17 shows the flow curves of four typical non-Newtonian fluids, including pseudo plastic, dilatant, Bingham and Herschel-Buckley fluids. Many constitutive equations have been developed to describe the flow of non-Newtonian fluid, which are shown as follows

Power law fluid:

$$\tau = K\dot{\gamma}^n \tag{11}$$

where K is the fluid consistency coefficient and n is called the flow behavior index representing the degree that the fluid deviates from the Newtonian fluid. $n < 1$ indicates that the viscosity decreases as the shear rate increases, therefore the fluid is shear thinning pseudo plastic fluid; $n > 1$ indicates that the viscosity increases as the shear rate increases, therefore the fluid is shear thickening dilatant fluid. Power law fluids are with zero yield stress, while Eq. (11) is re-written as follows when the yield stress is larger than zero,

Bingham fluid equation:

$$\tau = \tau_0 + \mu_0\dot{\gamma} \tag{12}$$

Herschel–Buckley fluid equation:

$$\tau = \tau_0 + K\dot{\gamma}^n \tag{13}$$

The above two equations are the descriptions of Bingham fluid and Herschel-Buckley fluid, respectively. Both fluids have yield stress $\tau_0 > 0$, however, after overcoming the yield stress, Bingham fluid behaves as Newtonian fluid and Herschel–Buckley fluid behaves as pseudo plastic fluid.

For the laminar flow in circular pipe, the shear stress varies linearly with radius:

$$\tau = \tau_w \frac{r}{R} = \frac{D\Delta P}{4l}\frac{r}{R} \tag{14}$$

where τ_w is the shear stress on the pipe wall. Then the volumetric flow rate is:

$$G = \int_0^R 2\pi r v \, dr = \pi \int_0^R r^2 \dot{\gamma} \, dr = \frac{\pi R^3}{\tau_w^3} \int_0^{\tau_w} \tau^2 \dot{\gamma} \, d\tau \tag{15}$$

The apparent viscosity on the wall is defined as:

$$\mu_a(\tau_w) = \frac{\tau_w}{\dot{\gamma}_w} \tag{16}$$

Shear rate on the pipe wall can be calculated by:

$$\dot{\gamma}_w = \frac{G}{\pi R^3}\left[3 + \frac{d\ln(G/\pi R^3)}{d\ln \tau_w}\right] = \frac{\dot{\gamma}_{wN}}{4}\left[3 + \frac{d\ln \dot{\gamma}_{wN}}{d\ln \tau_w}\right] \tag{17}$$

where $\dot{\gamma}_{wN}$ stands for the wall shear rate of Newtonian fluid, equaling $4G/\pi R^3$,

Define:

$$n = \frac{d\ln \tau_w}{d\ln \dot{\gamma}_{wN}} = \frac{d\ln(D\Delta P/4l)}{d\ln(8v/D)} \tag{18}$$

Then, for power law fluid:

$$\tau_w = K\dot{\gamma}_w^n = K'\dot{\gamma}_{wN}^n \tag{19}$$

Therefore, after obtaining the pressure drops and flow rates of CHS, the flow behavior index n can be identified by the slope of the fitting curve of $\ln(D\Delta P/4l)$ versus $\ln(8v/D)$.

For Bingham fluid, the Buckingham equation can be deduced from Eq. (15):

$$\frac{G}{\pi R^3} = \frac{\tau_w}{\mu_0}\left[\frac{1}{4} - \frac{1}{3}\frac{\tau_0}{\tau_w} + \frac{1}{12}\left(\frac{\tau_0}{\tau_w}\right)^4\right] \tag{20}$$

Neglecting higher order item of $(\tau_0/\tau_w)^4$, Eq. (20) can be written as:

$$\tau_w = \frac{4}{3}\tau_0 + \mu_0 \frac{8v}{D} \tag{21}$$

Thus, τ_0 and μ_0 can be obtained from the curve of $D\Delta P/4l$ versus $8v/D$.

Darbouret et al. [48] treated the TBAB CHS as Bingham fluid, and applied Eq. (21) to fitting the experimental data. And Hayashi et al. [49] measured the flow characteristics of 35, 29, 27 and 26 vol% TBAB CHS in the pipes with the inner diameters of 27.6 and 52.9 mm and the equation for power law fluid was used to fit the experimental data. Results of both works are shown in Fig. 18. It can be seen from the figure that results of Hayashi et al. seemed to vary significantly even with only a small change of volume fraction, and the apparent viscosity was larger than that obtained by Darbouret et al. at the same volume fractions.

As shown in Fig. 18, the results of Darbouret et al. indicated that there was a critical volume fraction for TBAB CHS at which its flow behavior changed from Newtonian fluid to Bingham fluid. However, the authors found that it was difficult to determine precisely the value of this critical point. Apparently, CHS in higher volume fraction has larger yield stress and apparent viscosity. It was further found that the viscosity of type B TBAB CHS was a little larger than that of type A due to the different shapes of two types of hydrate crystals. According to Darbouret et al., the yield stresses of both type A and type B CHS varied with ϕ^3.

Xiao et al. [50] tested the flow characteristics of TBAB CHS in a PVC pipe with 21 mm inner diameter. Power law fluid equation

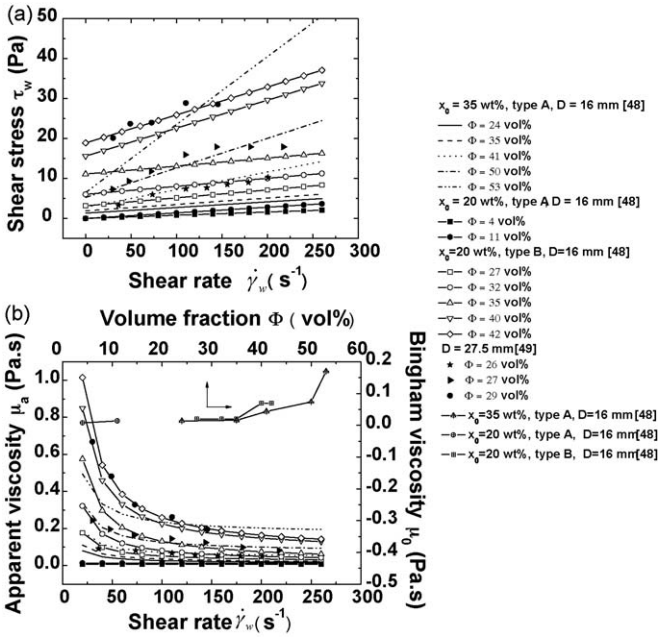

Fig. 18. Flow curves and apparent viscosities obtained by Darbouret et al. [48] and Hayashi et al. [49].

was applied, which showed that the apparent viscosity of 0–16 vol% TBAB CHS was only 3–8 times lager than that of water, much smaller than the results obtained by Darbouret et al. [48] and Hayashi et al. [49]. And a linear correlation between the flow behavior index n and volume fraction ϕ was proposed based on the experimental results:

$$n = -2.7\phi + 1 \tag{22}$$

Flow behavior of CHS may be affected by many factors, such as the shape and volume fraction of hydrate crystal particles, the pipe shape and size, and so on. It can be concluded from the different results given above that the flow characteristics of CHS are very complicated and still need more experimental and theoretical investigations.

3.3.2. Friction factor of CHS

Friction factor can also be calculated through measuring the pressure drop and flow rate. For power law fluids, Metzner and Reed [51] proposed a modified Reynolds number Re_{MR} as follows:

$$Re_{MR} = \frac{Dv\rho}{K}\left(\frac{4n}{3n+1}\right)^n \left(\frac{8v}{D}\right)^{1-n} = \frac{D^n v^{2-n}\rho}{K' 8^{n-1}} \tag{23}$$

Using this modified Reynolds number, the Fanning friction factor for the laminar flow of power law fluid can be calculated by the following equation which accords with that for the laminar flow of Newtonian fluid:

$$f = \frac{16}{Re_{MR}} \tag{24}$$

for the turbulent flow, only empirical or semi-empirical equations were available. Metzner [52] proposed an empirical equation in the similar form to Blasius equation for non-Newtonian turbulent flow:

$$f = \frac{a}{Re_{MR}^b} \tag{25}$$

where a and b are the function of the flow behavior index n, and both values are given in Table 5.

Table 5
Values of a and b in Eq. (25) [52].

N	a	b
0.2	0.0646	0.349
0.3	0.0685	0.325
0.4	0.0712	0.307
0.6	0.0740	0.281
0.8	0.0761	0.263
1.0	0.0779	0.250
1.4	0.0804	0.231
2.0	0.0828	0.213

Dodge and Metzner [53] also proposed a semi-empirical equation for the turbulent flow of power law fluid:

$$\frac{1}{\sqrt{f}} = \frac{4.0}{n^{0.75}} \log(Re_{MR} f^{\frac{2-n}{2}}) - \frac{0.4}{n^{1.2}} \tag{26}$$

For Bingham fluid in the laminar flow, the following equation can be derived from Eq. (20):

$$f = \frac{16}{Re_B}\left(1 + \frac{1}{6}\frac{He}{Re_B} - \frac{1}{3}\frac{He^4}{f^3 Re_B^3}\right) \tag{27}$$

where $Re_B = \rho v D/\mu_0$ stands for the Reynolds number for the Bingham fluid, and $He = D^2\rho\tau_0/\mu^2$ is the Hedstrom number. The highest order term in this equation can always be neglected.

Hayashi et al. [49] presented the results of f versus Re_{MR} by using Eq. (24), and Darbouret et al. [48] gave out the results of ΔP versus Re_B based on Eq. (27), and both authors claimed the good agreement between the calculated and experimental values. In the turbulent flow of CHS, Xiao et al. [50] claimed that both initial mass concentration of the aqueous solution and volume fraction of hydrate particles had little effect on the results of f and Re, and the following empirical equation was obtained from the experimental results:

$$f = 0.3226 Re_{MR}^{-0.4271} \tag{28}$$

In order to reduce the large frictional pressure drop of CHS flow, the drag-reduction surfactants are often added into the fluid. Suzuki et al. [54] applied oleylbishydroxyethylmethylammonium chloride [$C_{18}H_{35}N(C_2H_4OH)_2CH_3CCl$, trade name: ethoquad O/12] to TME CHS, and found that, however, the agent could only reduce the pressure drop of CHS with high solid fraction in the turbulent flow, and the heat transfer performance was reduced even more because of the suppression of the turbulence.

There are few results of CHS flow characteristics in the open literature. Recent experimental results (not published yet) obtained by a group at Shanghai Jiao Tong University (SJTU) showed that the flow of TBAB CHS displayed power law fluid feature. The flow test was conducted with a horizontal copper tube of 6 mm inner diameter. Flow behavior indexes of 5–20 vol% CHS were about 0.91–0.74 and varied little when the volume fraction further became larger. The experimental results for the turbulent flow state were also obtained and showed good agreement with Eq. (25) and Eq. (26), as shown in Fig. 19.

3.4. Heat transfer characteristics of CHS

Heat transfer tests of TBAB CHS were carried out by the researchers in JFE Corporation [55], in which a fan coil unit with a nominal flow rate of about 5 kg/min and 3.66 kW cooling capacity was used to study the heat transfer characteristics of TBAB CHS. The overall cooling load and mass flow rate were measured for both chilled water and CHS, consequently, the heat transfer coefficient h was obtained. An example of the results is shown in Fig. 20.

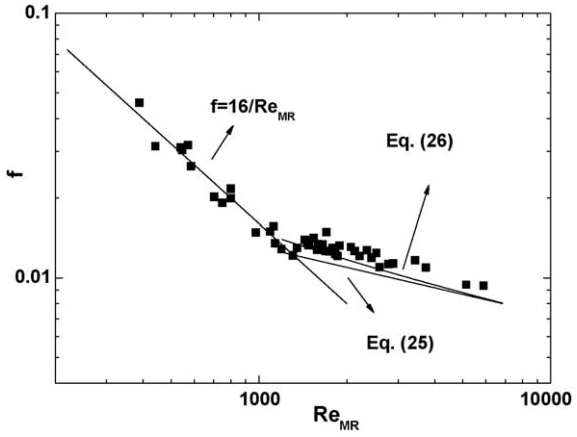

Fig. 19. f–Re_{MR} results of TBAB CHS obtained at SJTU.

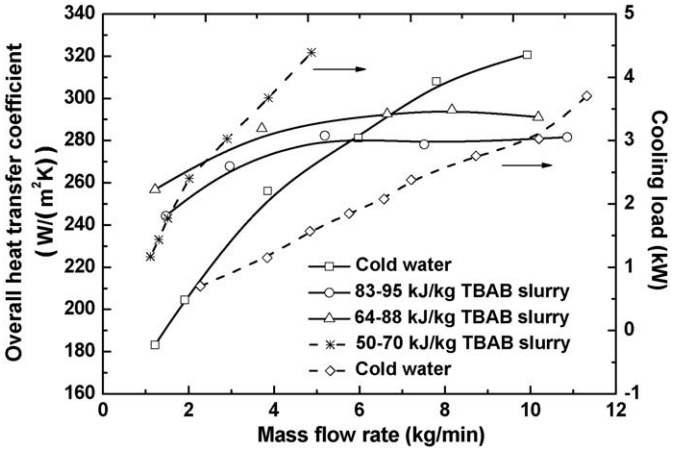

Fig. 20. Heat transfer performance and cooling capacity of CHS in a fan coil heat exchanger [55].

Compared to the chilled water, CHS exhibited a higher overall heat transfer coefficient due to the associated phase change, as shown in Fig. 20. However, large viscosity of CHS results in a low Reynolds number compared to water at the same flow rate, which consequently deteriorates the heat transfer performance. Results in Fig. 20 show the cooling capacity of TBAB CHS is about 2.5–3.5 times larger than that of the chilled water at the flow rate of 1–5 kg/min.

Xiao et al. [56] investigated the heat transfer characteristics of TBAB CHS in a horizontal copper tube with 8 mm inner diameter. They used the electric resistance as the heater, and the maximal heating power was 12 kW. The results indicated that the influence of the volume fraction of solid phase on Nusselt number was small despite the change of Reynolds numbers. A correlation of Nu with Re_{MR} was proposed as follows:

$$Nu = 0.2049 Re_{MR}^{0.6732} \tag{29}$$

It is obvious that the heat transfer characteristics data is very important for the system design and cooling power evaluation of CHS, thus, more data is still needed to facilitate this purpose.

It should be pointed out that the heat transfer of CHS flow in the tube is very complicated, which involves not only the variation of the volume fraction of solid phase and the consequent variation of the melting temperature of CHS but also the change of the flow characteristics of CHS because of its non-Newtonian fluid feature. The latter two difficulties are not involved in the case of MPCS. Furthermore, the fluid flow and heat transfer behaviors of CHS in

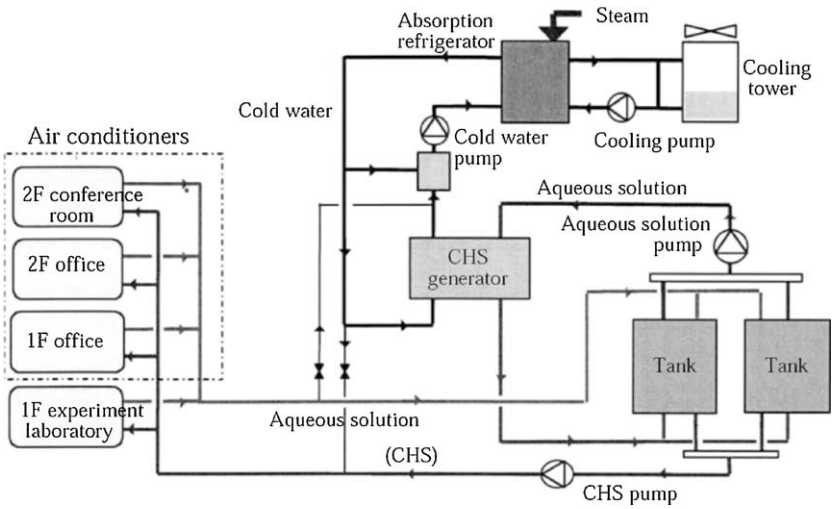

Fig. 21. The scheme of the air conditioning system using TBAB CHS [57].

the heat exchangers obviously urge more investigation on this topic as well.

3.5. Application of CHS to the refrigeration and air conditioning system at the industrial scale

An air conditioning system using TBAB CHS as both the cold storage and transportation media in the secondary refrigeration loop has been applied to an office building in NKK Keihin Workshop [57]. Shown in Fig. 21 is the schematic layout of the air conditioning system using TBAB CHS in which an absorption refrigerator was used to generate cold. A CHS generator was applied to generating TBAB CHS during the off-peak time, and the CHS was stored in one of the two tanks, as shown in Fig. 21. TBAB CHS was pumped directly to the load side by a special CHS pump during daytime to provide cooling, which resulted in the electricity peak-shaving. After passing the heat exchanger, TBAB CHS dissolved and became the aqueous solution which was then stored in another tank. However, if TBAB CHS could not suffice all the cold loads, the refrigerator would start to compensate.

Because of the involvement of CHS in the air conditioning system, the initial capital cost was reduced due to the capacity reduction of the refrigeration system and the size reduction of the pipes, and the operating cost was also reduced due to the reduction of the pumping power. The operation during the summer in the year of 2000 revealed that the pumping power consumption was reduced to 50% of that for chilled water system, and 21% of the overall power consumption was reduced.

4. Conclusions

An overview of MPCS and CHS used as the phase change material slurries (PCS) for the thermal storage and transportation has been carried out, which is presented by dividing into two big sections. The materials and fabrication methods suitable for MPCS and CHS have been presented, and the determination of the thermal properties of MPCS and CHS, like thermal conductivity, specific heat and viscosity, are also discussed. The flow characteristics are different for MPCS and CHS, which can be characterized by Newtonian fluid feature for MPCS with small solid volume fraction and by non-Newtonian fluid feature for CHS and MPCS with high solid volume fraction. The heat transfer of PCS with phase change is quite complicated, which still needs more intensive investigation. The application of PCS to the secondary loop as the thermal storage and transportation media is also presented, which is very promising for the practical application in the future.

References

[1] Fournaison L, Delahaye A, Chatti I, Petitet J. CO_2 hydrate in refrigeration processes. Industrial & Engineering Chemistry Research 2004;43(20):6521–6.
[2] Inaba H. New challenge in advanced thermal energy transportation using functionally thermal fluids. International Journal of Thermal Sciences 2000;39(9):991–1003.
[3] Hawlader MNA, Uddin MS, Khin MM. Microencapsulated PCM thermal-energy storage system. Applied Energy 2003;74(1–2):195–202.
[4] Jahns E. Microencapsulated phase change material. In: International Energy Agency. Energy Conversation through Energy Storage Program (ECES), Annex 10: Fourth Workshop; 1999.
[5] Alkan C, Sari A, Karaipekli A, Uzun O. Preparation, characterization, and thermal properties of microencapsulated phase change material for thermal energy storage. Solar Energy Materials and Solar Cells 2009;93(1):143–7.
[6] Jin ZG, Wang YD, Liu JG, Yang ZZ. Synthesis nd properties of paraffin capsultes as phase change materials. Polymer 2008;49(12):2903–10.
[7] Ai YF, Jin Y, Sun J, Wei DQ. Microencapsulation of n-hexadecane as phase change material by suspension polymerization. e-Polymers 2007;1–9. 98.
[8] Zou GL, Tan ZC, Lan XZ, Sun LX, Zhang T. Preparation and characterization of microencapsulated hexadecane used for thermal energy storage. Chinese Chemical Letters 2004;15(6):729–32.
[9] Li W, Zhang XX, Wang XC, Niu JJ. Preparation and characterization of microencapsulated phase change material with low remnant formaldehyde content. Materials Chemistry and Physics 2007;106(2–3):437–42.
[10] Özonur Y, Mazman M, Paksoyn HÖ, Evliya H. Microencapsulation of coco fatty acid mixture for thermal energy storage with phase change material. International Journal of Energy Research 2006;V30(19):741–9.
[11] Alvarado JL, Marsh C, Sohn C, Vilceus M, Hock V, Phetteplace G, Newell T. Characterization of supercooling suppression of microencapsulated phase change material by using DSC. Journal of Thermal Analysis and Calorimetry 2006;86(2):505–9.
[12] Fan YF, Zhang XX, Wang XC, Li J, Zhu QB. Super-cooling prevention of microencapsulated phase change material. Thermochimica Acta 2004;413:1–6.
[13] Zhang XX, Tao XM, Yick KL, Wang XC. Structure and thermal stability of microencapsulated phase-change materials. Colloid and Polymer Science 2004;282:330–6.
[14] Guyer EC, Brownell DL. Handbook of applied thermal design. New York: McGraw-Hill; 1998.
[15] Charunyakorn P, Sengupta S, Roy SK. Forced convection heat transfer in microencapsulated phase change material slurries: flow in circular ducts. International Journal of Heat and Mass Transfer 1991;34(3):819–33.
[16] Wang XC, Niu JL, Li Y, Zhang YP, Wang X, Chen BJ, Zeng RL. Heat transfer of microencapsulated PCM slurry flow in a circular tube. AIChE Journal 2008;54(4):1110–20.
[17] Yamagishi Y, Takeuchi H, Pyatenko AT, Kayukawa N. Characteristics of microencapsulated PCM slurry as a heat-transfer fluid. AIChE Journal 1999;45(4):696–707.
[18] Vand V. Theory of viscosity of concentrated suspensions. Nature 1945;155:364–5.
[19] Goel M, Roy SK, Sengupta S. Laminar forced convection heat transfer in microcapsulated phase change material suspensions. International Journal of Heat and Mass Transfer 1994;37(4):593–604.

[20] Inaba H, Kim MJ, Horibe A. Melting heat transfer characteristics of microencapsulated phase change material slurries with plural microcapsules having different diameters. ASME Journal of Heat Transfer 2004;126(4):558–65.
[21] Alvarado JL, Marsh C, Sohn C, Phetteplace G, Newell T. Thermal performance of microencapsulated phase change material slurry in turbulent flow under constant heat flux. International Journal of Heat and Mass Transfer 2007;50(9–10): 1938–52.
[22] Zhao ZN, Hao R, Shi Y. Parametric analysis of enhanced heat transfer for laminar flow of microencapsulated phase change suspension in a circular tube with constant wall temperature. Heat Transfer Engineering 2008;29(1):97–106.
[23] Diaconu BM. Transient thermal response of a PCS heat storage system. Energy and Buildings 2009;41(2):212–9.
[24] Yamagishi Y, Sugeno T, Isi-iige T, Takeuci-ii H, Pyatenko AT. An evaluation of microencapsulated pcm for use in cold energy transportation medium. In: Energy Conversion Engineering Conference, IECEC 96. Proceedings of the 31st Intersociety; 1996. p. 2077–83.
[25] Wang XC, Niu JL, Van Paassen AHC. Raising evaporative cooling potentials using combined cooled ceiling and MPCM slurry storage. Energy and Buildings 2008;40(9):1691–8.
[26] Balikowski JR, Mollendor JC. Performance of phase change materials in a horizontal annulus of a double-pipe heat exchanger in a water-circulating loop. ASME Journal of Heat Transfer 2007;129(3):265–72.
[27] Griffiths PW, Eamesa PC. Performance of chilled ceiling panels using phase change material slurries as the heat transport medium. Applied Thermal Engineering 2007;27(10):1756–60.
[28] Fossett AJ, Kudirka AA, Kudirka AA. Avionics passive cooling with microencapsulated phase change materials. ASME Journal of Electronic Packaging 1998;120:238–42.
[29] Shibutani S. PCM Application in Narita Airport. In: Proceedings of 3rd Experts Meeting and Workshop of IEA; 2002 [Annex 17].
[30] Gschwander S, Schossig P, Henning H-M. Micro-encapsulated paraffin in phase-change slurries. Solar Energy Materials and Solar Cells 2005;85(2–3):307–15.
[31] Fowler DL, Loebenstein WV, Pall DB, Kraus CA. Some unusual hydrates of quaternary ammonium salts. Journal of the American Chemical Society 1940;62(5):1140–2.
[32] Lipkowski J, Komarov VY, Rodionova TV, Dyadin YA, Aladko LS. The structure of tetrabutylammonium bromide hydrate $(C_4H_9)_4NBr{\cdot}21/3H_2O$. Journal of Supramolecular Chemistry 2002;2:435–9.
[33] Kamata Y, Oyama H, Shimada W. Gas separation method using Tetra-*n*-butyl Ammonium Bromide semi-clathrate hydrate. Japanese Journal of Applied Physics 2004;43(1):362–5.
[34] Duc NH, Chauvy F, Herri JM. CO_2 capture by hydrate crystallization—A potential solution for gas emission of steelmaking industry. Energy Conversion and Management 2007;48:1313–22.
[35] Oyama H, Shimada W, Ebinuma T, Kamata Y, Takeya S, Uchida T, Nagao J, Narita H. Phase diagram, latent heat, and specific heat of TBAB semiclathrate hydrate crystals. Fluid Phase Equilibria 2005;234:131–5.
[36] Shimada W, Ebinuma T, Oyama H, Kamata Y, Narita H. Free-growth forms and growth kinetics of tetra-n-butyl ammonium bromide semi-clathrate hydrate crystals. Journal of Crystal Growth 2005;274:246–50.
[37] Nakayama H. Hydrates of organic compounds. VI. Heats of fusion and of solution of quaternary ammonium halide clathrate hydrates. Bulletin of the Chemical Society of Japan 1987;55:389–93;
Hydrates of organic compounds. XI: Determination of the melting point and hydration numbers of the clathrate-like hydrate of tetrabutylammonium chloride by differential scanning calorimetry. Bulletin of the Chemical Society of Japan 1987;60:839–43.
[38] Rodionova TV, Manakov AY, Stenin YG, Villevald GV, Karpova TD. The heats of fusion of tetrabutylammonium fluoride ionic clathrate hydrates. Journal of Inclusion Phenomena and Macrocyclic Chemistry 2008;61:107–11.
[39] Yamazaki M, Sasaki C, Kakiuchi H, Osano YT, Suga H. Thermal and structural characterization of trimethylolethane trihydrate. Thermochimica Acta 2002; 387:39–45.
[40] Dyadin YA, Udachin KA. Clathrate formation in water-peralkylonium salts systems. Journal of Inclusion Phenomena 1984;2:61–72.
[41] Arjmandi M, Chapoy A, Tohidi B. Equilibrium data of hydrogen, methane, nitrogen, carbon dioxide, and natural gas in semi-clathrate hydrates of tetrabutyl ammonium bromide. Journal of Chemical & Engineering Data 2007;52: 2153–8.
[42] Delahaye A, Fournaison L, Marinhas S, Chatti I. Effect of THF on equilibrium pressure and dissociation enthalpy of CO_2 hydrates applied to secondary refrigeration. Industrial & Engineering Chemistry Research 2006;45:391–7.
[43] Lin W, Delahaye A, Fournaison L. Phase equilibrium and dissociation enthalpy for semi-clathrate hydrate of CO2 +TBAB. Fluid Phase Equilibria 2008;264:220–7.
[44] Li DL, Du JW, Fan SS, Liang DQ, Li XS, Huang NS. Clathrate dissociation conditions for methane + tetra-*n*-butyl ammonium bromide (TBAB) + water. Journal of Chemical & Engineering Data 2007;52:1916–8.
[45] Takao S, Ogoshi H, Fukushima S, Matsumoto S. Thermal storage medium using a hydrate and apparatus thereof, and method for producing the thermal storage medium. United States Patent Application Publication. US Patent 7,246,506; 2007, B2.
[46] Wu SS, Xiao R, Huang C, Tang LG, Feng ZP, Fan SS. Research on clathrate hydrate of Tetra-n-butylammonium Bromide as cold-storage material in air-conditioning. Journal of Refrigeration 2006;27(6):48–51. In Chinese.
[47] Daitoku T, Utaka Y. An effect of scraper shapes on detachment of solid adhered to cooling surface for formation of clathrate hydrate slurry. Heat Transfer-Asian Research 2007;36:489–500.
[48] Darbouret M, Cournil M, Herri JM. Rheological study of TBAB hydrate slurries as secondary two-phase refrigerants. International Journal of Refrigeration 2005;28:663–71.
[49] Hayashi K, Takao S, Ogoshi H, Matsumoto S. Research and development on high-density cold latent-heat medium transportation technology. In: Fifth Workshop, Final Proceedings; 2000. p. 1–9 [PPIEA, Annex 10].
[50] Xiao R, Wu SS, Tang LG, Huang C, Feng ZP. Experimental investigation of the pressure-drop of clathrate hydrate slurry (CHS) flow of tetrabutylammonium bromide (TBAB) in straight pipe. In: Proceedings of 10th International Conference on Thermal Energy Storage; 2006.
[51] Metzner AB, Reed JC. Flow of non-newtonian fluids—correlation of the laminar, transition, and turbulent-flow regions. AIChE Journal 1955;1(4):434–40.
[52] Metzner AB. Recent developments in the engineering aspects of rheology. Rheologica Acta 1958;1:205–12.
[53] Dodge DW, Metzner AB. Turbulent flow of non-Newtonian systems. AIChE Journal 1959;5(2):189–204.
[54] Suzuki H, Itotagawa T, Indartono YS, Usui H, Wada N. Rheological characteristics of trimethylolethane hydrate slurry treated with drag-reducing surfactants. Rheologica Acta 2006;46:287–95.
[55] Ogoshi H, Takao S. Air-conditioning system using clathrate hydrate slurry. JFE Technical Report 2004;(3):1–5.
[56] Xiao R, He SH, Huang C, Feng ZP, Fan SS. Convectional heat transfer of TBAB clathrate hydrate slurry flow in copper tube. Journal of Chemical Industry and Engineering 2007;58(9):2205–10 [in Chinese].
[57] Takao S, Ogoshi H, Matsumoto S, Takashi K, Sugiyama M, Akiyama T, Fukushima S. New air conditioning systems using hydrate slurry. NKK Technical Report 2001;(174):6–11 [in Japanese].